

Self-Assembly of Ge and GaAs Quantum Dots under Tensile Strain on InAlAs(111)A

Kathryn E. Sautter,¹ Christopher F. Schuck,¹ Justin C. Smith, Kevin D. Vallejo, Trent A. Garrett, Jake Soares, Hunter J. Coleman, Michael M. Henry, Eric Jankowski, Christian Ratsch, and Paul J. Simmonds^{*}



Cite This: *Cryst. Growth Des.* 2021, 21, 1674–1682



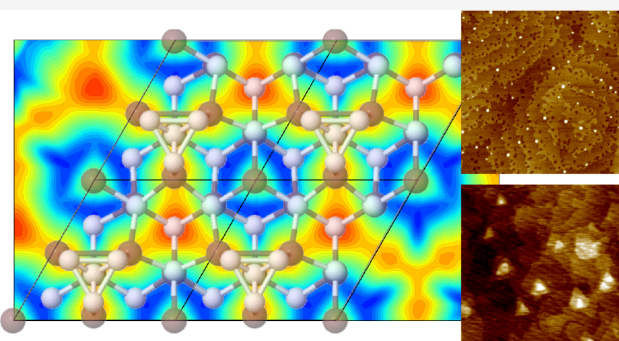
Read Online

ACCESS |

Metrics & More

Article Recommendations

ABSTRACT: Quantum dots that store large tensile strains represent an emerging research area. We combine experiments and computational modeling to investigate the self-assembly of Ge and GaAs tensile-strained quantum dots (TSQDs) on $\text{In}_{0.52}\text{Al}_{0.48}\text{As}$ (111)A. Comparing these two nominally similar material systems highlights how differences in adatom kinetics leads to distinct features of Ge and GaAs TSQD self-assembly. The energy barrier to diffusion of Ge adatoms is higher than that for Ga adatoms, while forming a stable island requires six Ge atoms and four Ga atoms. Unusually, these critical cluster sizes do not increase as we raise the substrate temperature. Radial distribution scaling shows that both Ge and GaAs TSQDs preferentially nucleate at a particular distance from their neighbors. This deeper understanding of the physics of Ge(111) and GaAs(111)A TSQD self-assembly will enable researchers to more effectively tailor these nanostructures to specific optoelectronic applications.



I. INTRODUCTION

Demand is growing for high-quality semiconductor materials with a (111) crystallographic orientation. The structural and electronic characteristics of (111) surfaces give rise to properties that are inaccessible to semiconductors with the traditional (001) orientation. (111)-Oriented semiconductor heterostructures are attractive for applications including topological insulators,^{1–3} transition metal dichalcogenides and other 2D materials,^{4–6} optoelectronics based on strain-induced piezoelectric effects,^{7,8} and next-generation field-effect transistors.^{9,10}

Quantum nanostructures grown on (111) surfaces exhibit some unique characteristics. Since tensile rather than conventional compressive strain is required to drive their self-assembly, these quantum dots (QDs) and quantum dashes derive their properties from both an unusual strain state and an unusual surface orientation.^{11–17} For example, we can create defect-free Ge QDs on InAlAs(111)A (hereafter Ge(111)) under tensile strains $\geq 3.5\%$,¹⁷ an important step toward future direct band gap Ge-based light emitting devices.^{17–21} Tensile strain lifts the valence band degeneracy, pushing the light-hole states of a tensile-strained QD (TSQD) above its heavy-hole states, with important implications for quantum media conversion.^{22,23} Meanwhile, the high symmetry of the (111) surface produces GaAs QDs with low fine-structure splitting,

ideally suited to entangled photon generation via the biexciton–exciton decay cascade.^{14,24,25}

However, the ability to grow these nanostructures is still in its infancy. A solid physical foundation for this emerging research field is needed to provide a clearer understanding of how TSQDs form and grow on (111) surfaces. By comparing the Ge(111) and GaAs(111)A TSQD systems, we have an opportunity to explore this developing growth technique at the atomic level. Ge and GaAs TSQDs are grown on $\text{In}_{0.52}\text{Al}_{0.48}\text{As}$ (111)A (hereafter InAlAs), lattice-matched to InP.^{15–17} The substrate temperatures and growth rates used during molecular beam epitaxy (MBE) are broadly similar for Ge and GaAs TSQDs. The major difference between the two materials is polarity: Ge is nonpolar, while GaAs is a polar, compound semiconductor. However, from the point of view of the underlying InAlAs(111)A surface structure and tensile strain, these two TSQD systems are analogous. The almost identical lattice constants of Ge (5.6579 Å) and GaAs (5.6533 Å) mean

Received: November 11, 2020

Revised: February 1, 2021

Published: February 12, 2021



that both materials experience $\sim 3.7\%$ tensile lattice mismatch with InAlAs. Removing these commonalities of surface structure and strain from the equation gives us a clearer view of the other physical factors influencing how TSQDs form and grow.

In this paper we show that TSQD self-assembly in these nominally similar Ge/InAlAs(111)A and GaAs/InAlAs(111)A materials systems exhibits some interesting and important differences. Density-functional theory (DFT) calculations reveal enhanced surface mobility for Ga adatoms compared to Ge. This study provides insight into the underlying kinetic processes that govern tensile-strained self-assembly during TSQD nucleation and growth. By comparing the scaled size and radial distributions of Ge and GaAs TSQDs, we see opportunities to enhance the size uniformity and spatial ordering of these nanostructures for future device applications.

II. EXPERIMENTAL METHODS

We used Fe-doped, nominally on-axis ($\pm 0.5^\circ$) InP(111)A substrates for all sample growth. We grew samples via solid-source MBE, using As₄ as the group V source. We started by growing 50 nm of lattice-matched In_{0.52}Ga_{0.48}As (hereafter InGaAs) at 169 nm/h to promote smoother InAlAs epitaxy.²⁶ We then grew 200 nm InAlAs at 172 nm/h as a bottom barrier for the Ge and GaAs TSQDs. We grew both InGaAs and InAlAs at a substrate temperature (T_{sub}) of 510 °C, with a V/III beam equivalent pressure (BEP) ratio of 160. Optimized MBE growth conditions for InGaAs and InAlAs on InP(111)A are discussed elsewhere.^{15,26,27}

To grow the Ge TSQDs, we adjusted T_{sub} for TSQD growth under As₄, closed the arsenic shutter and valve, waited 1 min, and then opened the Ge shutter.¹⁷ Previous studies have shown that the InAlAs(111)A surface is thermally stable at these temperatures, even when the arsenic flux is removed for a short time.^{17,28} For the GaAs TSQDs, we adjusted the sample to the desired T_{sub} for TSQD growth under an As₄ flux and then opened the Ga shutter.¹⁵

In this study, we looked at four sets of samples: Ge TSQDs consisting of 0.2–0.6 bilayers (BL) of Ge grown at $T_{\text{sub}} = 535$ and 560 °C, and GaAs TSQDs consisting of 3.5–4.5 monolayers (ML) of GaAs grown at $T_{\text{sub}} = 485$ and 535 °C. The Ge growth rate was 0.020 BL/s. The GaAs growth rate was 0.075 ML/s, with an As₄/Ga BEP ratio of 75. After TSQD growth, we immediately cooled the samples; for the GaAs TSQDs, sample cooling took place under As₄.

We imaged the Ge and GaAs TSQDs with atomic force microscopy (AFM), using Nanoscope software to measure the height and diameter of 100–200 individual TSQDs on each sample. From these measurements, we compiled sample-dependent statistics of TSQD size distribution and areal density, which we used for island size scaling analysis. We used ImageJ software²⁹ to identify the TSQD coordinate positions on each AFM image. From these coordinates, we used a Python script and the *freud* analysis library³⁰ to extract interdot distances and plot the radial distribution of TSQDs on each sample.

III. COMPUTATIONAL METHODS

All electronic structure calculations were performed using DFT,^{31,32} as implemented in the Fritz Haber Institute *ab initio* molecular simulations (FHI-aims) code.^{33–36} FHI-aims uses numeric atom-centered orbitals for its basis set and by default includes scalar relativistic corrections. For all calculations, we used the Perdew–Burke–Ernzerhof generalized gradient approximation for the exchange-correlation (XC) approximation.³⁷ FHI-aims implements “light” and “tight” versions of its basis functions. We use the light settings throughout. Tight settings yield more accurate energies but do not change energy differences, which is our interest here.

To simulate a bulk random alloy such as InAlAs, a method such as special quasirandom structures (SQS) must be

used.^{38,39} However, we found that our calculations can be simplified by using InAs that is compressed 3.13% to the lattice constant of In_{0.52}Al_{0.48}As (i.e., 5.8687 Å). We justify this simplification with DFT calculations for InAs and AlAs strained to have the same lattice constant as In_{0.52}Al_{0.48}As-(111)A. We calculate that the InAs(111)A surface energy is lower than that of AlAs(111)A by ~ 70 meV/Å², which corresponds to ~ 1.2 eV per surface atom. We also ran a series of calculations for In_{0.5}Al_{0.5}As(111)A in three scenarios: (i) we fixed the top two group III layers as In; (ii) we fixed the top two group III layers as Al; and (iii) we maintained a 50–50 mix of In and Al in the top two layers. In all cases, the remaining group III atoms in the lower layers were randomized as In or Al (maintaining overall stoichiometry). These tests again show that the In-terminated surfaces are lower in energy than the Al-terminated surfaces by approximately 70 meV/Å². The In-terminated surfaces were also lower in energy than the surfaces with a 50–50 mix of In and Al by approximately 10–15 meV/Å². For all three cases, run-to-run variations between the different randomizations were 2–3 meV/Å². Furthermore, we find that the difference in adsorption energy for an adatom on these three surfaces is very small. Even for the extreme case with only Al atoms in the layers below the top two InAs layers, the adsorption energy changes by ≤ 60 meV, and adsorption energy differences (i.e., diffusion barriers) change by even less. As a result of these calculations, we therefore conclude that InAs not only surface segregates, but the atomic composition of the bulk InAlAs below the top few layers has minimal bearing on the results at the surface.

Supporting our simulations is the fact that, during epitaxial growth of InAlAs(001) and InGaAs(001), the propensity for surface segregation of group III species increases with atomic size (i.e., In > Ga > Al).^{40,41} To confirm this effect in our (111)A-oriented alloys, we use X-ray photoelectron spectroscopy (XPS) to construct elemental depth profiles for samples of InGaAs(111)A and observe a clear increase (decrease) in the surface concentration of indium (gallium) over the first 1–2 ML of the sample (Figure 1a). Equivalent XPS measurements for the InAlAs(111)A surface are complicated by oxidation in uncapped aluminum-containing alloys. However, since the observed effect is expected to be even stronger in In_{0.52}Al_{0.48}As than in In_{0.53}Ga_{0.47}As,⁴⁰ we have little doubt that

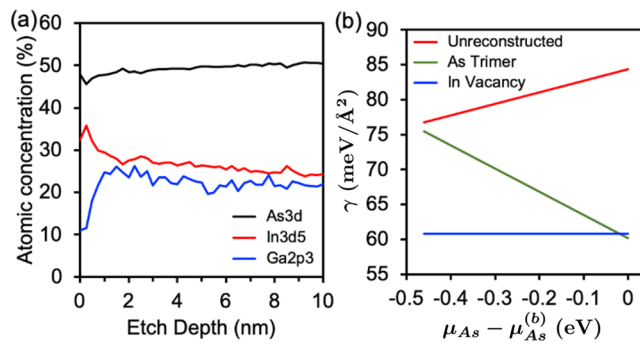


Figure 1. (a) XPS depth profile of bulk In_{0.53}Ga_{0.47}As(111)A showing enrichment (depletion) of indium (gallium) at the surface. (b) Surface energy of 3.13% compressively strained InAs versus arsenic chemical potential for both 2 × 2 reconstructions and the unreconstructed surface. The x-axis is equivalent to controlling the arsenic overpressure but is by no means one-to-one with an experimental knob.

the results of our simulations are correct and that In surface segregation occurs in InAlAs(111)A.

The InAs(111)A surface is indium-terminated and has an AB–AB–AB pattern. Two stable reconstructions exist for the InAs(111)A surface: an indium-vacancy and an arsenic-trimer reconstruction, both of which have a 2×2 unit cell (Figure 1b). We limit our calculations to these two surface reconstructions. All our results are converged with respect to layers of vacuum (30 Å), k points ($6 \times 6 \times 1$ k points for 2×2 supercells and $12 \times 12 \times 1$ k points for regular 1×1 cells) and slab thickness (five BL). We cap the final bottom layer with pseudohydrogen to minimize interaction with the top surface. Each bilayer contains 8 atoms in a 2×2 cell, and a typical calculation with a 2×2 cell for an adatom on the indium-vacancy (arsenic-trimer) reconstruction contains 43 (47) atoms total.

In Figure 1b, we plot the phase diagram for the compressively strained InAs(111)A surface energy versus the arsenic chemical potential, which one can interpret physically as the arsenic overpressure during MBE (albeit with a nonlinear scaling to experimental settings). We find that the In-vacancy reconstruction is stable for lower arsenic overpressures, while the As-trimer reconstruction is stable for higher arsenic overpressures. These results are consistent with similar calculations for GaAs(111)A.⁴²

The first step for understanding QD formation and growth is to understand the mobility of adatoms on a given surface reconstruction. For example, a higher adatom mobility implies that the spacing between nuclei (that evolve into QDs) will increase. Although it seems reasonable to assume we have an As-trimer surface reconstruction given the high V/III flux ratio during MBE growth (Figure 1b), we could not confirm experimentally which reconstruction was present in all of our growths. We therefore calculated potential energy surfaces (PESs) for Ge and Ga adatoms on both the In-vacancy and As-trimer reconstructions of the InAs(111)A surface. As we will show, our conclusions regarding relative adatom mobility are qualitatively the same for both surface reconstructions. We obtained each PES by sampling a sufficiently large number of sites guided by test calculations that used the growing string⁴³ and climbing image methods,⁴⁴ implemented in aimsChain, a Python package included with FHI-aims.

IV. RESULTS AND DISCUSSION

A. Key Differences between Ge and GaAs TSQDs.

Despite self-assembling on nominally identical InAlAs(111)A surfaces, under similar MBE conditions, Ge and GaAs TSQDs exhibit major differences in size, shape, and areal density (Figure 2). Ge(111) TSQDs are lens shaped (Figure 2a) and are typically 0.5–3 nm high and 15–45 nm in diameter, with areal densities of 5×10^9 to $5 \times 10^{10} \text{ cm}^{-2}$ (Figure 2b).¹⁷ In contrast, GaAs TSQDs grown at the same T_{sub} self-assemble as equilateral triangles, reflecting the 3-fold symmetry of the (111)A surface (Figure 2c).^{14–16,28} GaAs TSQDs form as stacked, concentric monolayer-high islands terminated by “A-steps” perpendicular to the [211], [12̄1], and [112] directions,²⁸ rather than the high-index side-facets typical of InAs/GaAs(001) QDs.⁴⁵ The GaAs TSQDs are 0.7–2 nm high and 45–60 nm in diameter, with areal densities of 2×10^8 to $2 \times 10^9 \text{ cm}^{-2}$ (Figure 2d).^{15,16}

At $T_{\text{sub}} \geq 535^\circ\text{C}$, Ge TSQDs self-assemble directly on the InAlAs(111)A buffer via the Volmer–Weber (VW) growth mode.¹⁷ The InAlAs surface consists of rounded wedding cake-

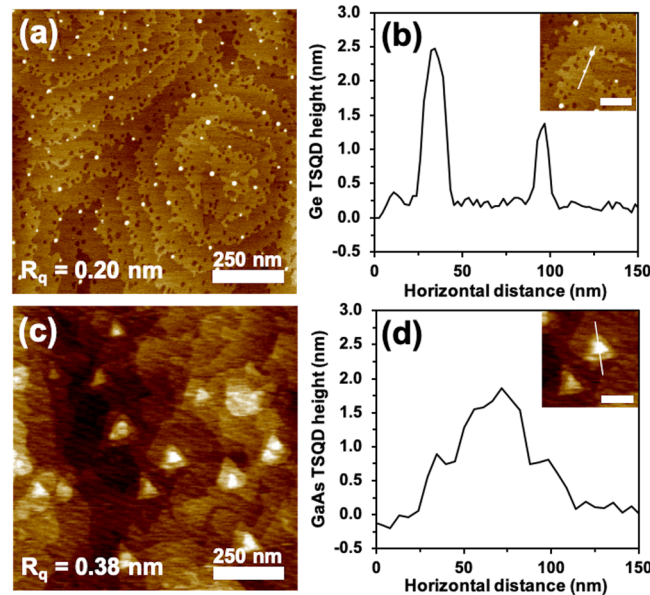


Figure 2. (a) AFM image showing typical Ge/InAlAs(111)A TSQDs, here grown from 0.2 BL Ge at $T_{\text{sub}} = 535^\circ\text{C}$. (b) Cross section showing height and diameter of two representative Ge(111) TSQDs. (c) AFM image showing typical GaAs/InAlAs(111)A TSQDs here grown from 4 ML GaAs at $T_{\text{sub}} = 535^\circ\text{C}$. (d) Cross section showing height and diameter of a representative GaAs(111)A TSQD. (insets b and d) AFM cross sections, where the white scale bars are 100 nm. The z-scale in all AFM images is 2.5 nm.

like terraces, 86 ± 13 nm wide (Figure 2a), with root mean squared roughness, $R_q \sim 2.0$ Å. The Ge TSQDs preferentially nucleate at the step edges connecting these terraces, as discussed in a previous report.¹⁷ Since the areal density of the Ge TSQDs is related to the number of available step edges, the use of off-cut substrates to adjust the step edge density represents a potential route to controlling TSQD density. In addition, TSQD density along a step edge is a function of the adatom diffusivity along that step edge, and the stability of small clusters (or the adatom binding energy) at the step edge. DFT studies of edge atom diffusion, binding energies, and cluster stability at step edges are computationally demanding and will form the subject of future work.

At comparable substrate temperatures, GaAs TSQDs self-assemble via an anomalous Stranski–Krastanov (SK) growth mode, where the tensile-strained GaAs wetting layer continues to grow even after the critical thickness for TSQD formation has occurred.¹⁶ The tensile-strained GaAs wetting layer exhibits angular terraces, 85 ± 26 nm wide, with $R_q \sim 3.8$ Å (Figure 2c). After the 2D-to-3D SK transition, the GaAs TSQDs nucleate randomly across the wetting layer surface, without preference for particular locations.^{15,16}

B. DFT Results for Surface Diffusion. To help us understand these differences in Ge and GaAs TSQD self-assembly, we use DFT calculations to compare adatom diffusion in the two material systems. Figure 3 shows the PES for Ge and Ga adatoms on the In-vacancy reconstruction. The energy barrier for surface diffusion, E_D , is given by the difference between the deepest energy well and the highest energy barrier as determined from exploring the PES. The adsorption site for both Ge and Ga atoms on the In-vacancy reconstruction is the vacancy site, labeled A_1 . For both systems, diffusion occurs via a path that passes through a shallow

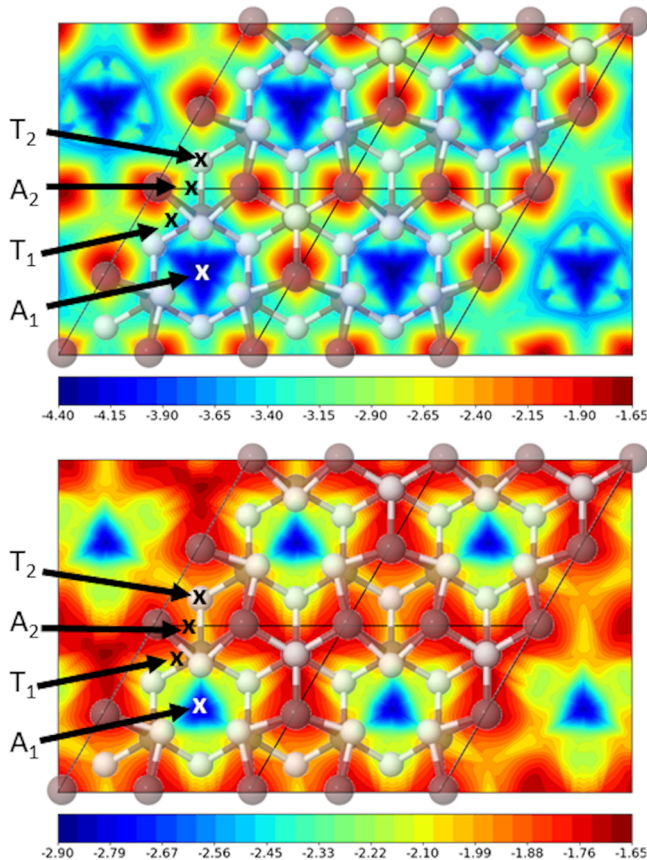


Figure 3. Potential energy surfaces for Ge (top) and Ga (bottom) adsorbed on the compressed In-vacancy reconstruction. The dark atoms are In, and the light atoms are As. The main adsorption site A_1 , a secondary shallow minimum A_2 , and the two transition sites T_1 and T_2 are shown.

secondary minimum (labeled A_2) and two transition sites (T_1 and T_2). We hence calculate the energy barrier to diffusion as $E_D = T_1 - A_1$. The adsorption energies and diffusion barriers for Ge and Ga on the In-vacancy reconstruction are summarized in Table 1. Since E_D is lower for Ga than Ge, Ga adatoms will diffuse faster than Ge adatoms on the In-vacancy surface.

Table 1. Adsorption Parameters for Ge and Ga on the In-Vacancy Reconstruction of the (Compressed) InAs(111)A Surface^a

adatom	A_1	A_2	T_1	T_2	E_D
Ge	-4.36	-3.59	-3.09	-3.23	1.27
Ga	-2.82	-2.04	-1.92	-1.97	0.90

^aWe list the primary adsorption energy A_1 , secondary adsorption energy A_2 , the higher transition site energy barrier T_1 , and the lower transition energy barrier T_2 , as shown in Figure 3. All values are in eV.

Figure 4 shows the PES for Ge and Ga adatoms on the As-trimer reconstruction. For this surface, there are two almost degenerate adsorption sites, labeled A_1 and A_2 , in the region centered between three adjacent As trimers. There is almost no barrier for diffusion between A_1 and A_2 for Ga, and only a small diffusion barrier for Ge. We therefore refer to this region as a *superbasin*. Both Ge and Ga adatoms diffuse to the next superbasin by passing over an As trimer, but the details for Ge

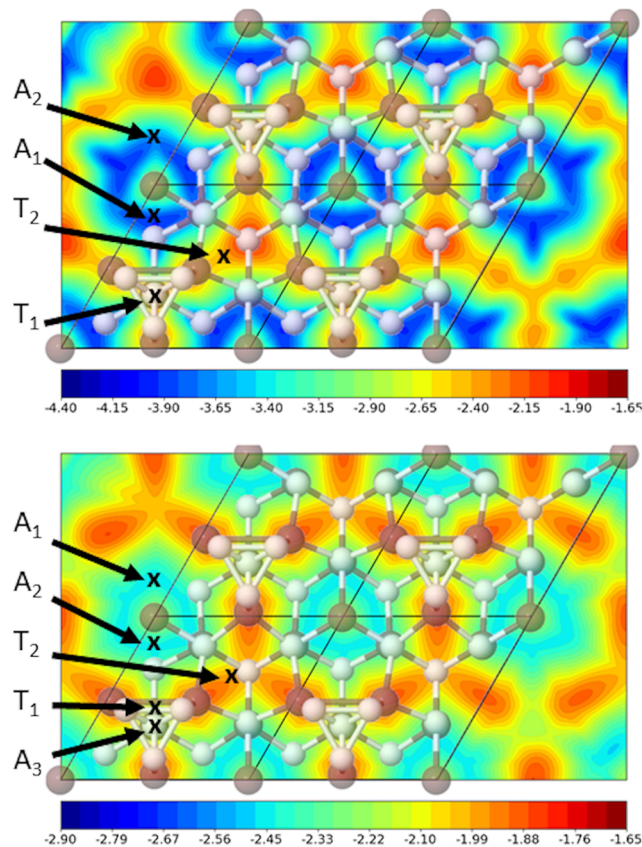


Figure 4. Potential energy surfaces for Ge (top) and Ga (bottom) adsorbed on the compressed As-trimer reconstruction. The dark atoms are In, and the light atoms are As. The main adsorption sites A_1 and A_2 , a secondary shallow minimum A_3 , and the transition sites T_1 and T_2 are shown.

and Ga are slightly different. For Ge, the transition site T_1 is in the center of the As trimer. For Ga, on the other hand, there is a secondary adsorption site A_3 in the center of the trimer, and the transition site T_1 is on top of an As dimer bond within the As trimer. For both Ge and Ga, a secondary transition site T_2 provides an alternative path for diffusion. For Ge, the two diffusion paths are almost degenerate, while for Ga, the path via T_2 is 0.15 eV higher than T_1 . The numerical values for Ge and Ga for all these sites and the barrier for surface diffusion are summarized in Table 2. The lower E_D for Ga means that Ga diffusion is again much faster than Ge diffusion on the As-trimer surface.

We note that due to the SK growth mode, the GaAs TSQDs begin to form only after the deposition of a few 2D layers of GaAs. Diffusion of Ga adatoms on this tensile-strained GaAs

Table 2. Adsorption Parameters for Ge and Ga on the As-Trimer Reconstruction of the (Compressed) InAs(111)A Surface^a

adatom	A_1	A_2	A_3	T_1	T_2	E_D
Ge	-4.18	-3.90	n/a	-2.72	-2.69	1.46
Ga	-2.72	-2.71	-2.48	-2.44	-2.29	0.28

^aWe list the main adsorption energies A_1 and A_2 , a secondary adsorption energy A_3 , the higher transition site energy barrier T_1 , and the lower transition energy barrier T_2 , as shown in Figure 4. All values are in eV.

wetting layer (i.e., its in-plane lattice constant expanded to that of the underlying InAlAs) is hence the relevant process in this case. We therefore performed corresponding DFT calculations for Ga on 1 ML (2 ML) of tensile-strained GaAs on InAs(111)A (compressed to have the InAlAs lattice constant as before). We find that the Ga adatom diffusion barrier is then 1.10 eV (1.24 eV) for the In-vacancy reconstruction (which is now a Ga-vacancy reconstruction),⁴² and 0.10 eV (0.10 eV) for the As-trimer reconstruction. Comparing these barriers with those in Tables 1 and 2 tells us that Ga diffusion on a thin GaAs(111)A wetting layer is still faster than Ge, and so our conclusions remain unchanged. We also note that these diffusion barriers for Ga on 1–2 ML of tensile-strained GaAs(111)A are similar to values we have obtained previously for Ga on unstrained GaAs(111)A, suggesting that the presence of strain does not modify the differences between Ga and Ge diffusion behavior to a great extent.⁴⁶

The fact that for a given T_{sub} , Ga diffuses faster than Ge means that diffusivity arguments alone are unable to explain our experimental observation that Ge TSQDs form predominantly at the step edges, while GaAs TSQDs form on the terraces (Figure 2). We speculate that small GaAs clusters are more stable than small Ge clusters. GaAs clusters are sufficiently stable that they can form directly on the terraces, while dangling bonds available at the step edges are needed to help stabilize Ge clusters. Step edges play a more important role for Ge since unlike GaAs it can fill both group III and group V sites and still satisfy electron counting rules. We believe that this difference in bonding between group III and group IV atoms is ultimately the main reason for the distinct self-assembly behaviors of Ge and GaAs TSQDs. However, future experiments to compare other group IV and III–V TSQD systems, for example Si and GaP TSQDs grown on GaAs(111)A,¹¹ could allow us to definitively rank the relative importance to self-assembly of differences in adatom diffusion vs differences in bonding.

C. Scaling of Ge and GaAs TSQD Size Distributions.

To experimentally test this hypothesis of differences in cluster stability, we studied the scaled island size distribution functions for Ge and GaAs TSQDs. This scaling analysis allows one to identify how many atoms are required to stabilize a cluster and nucleate a TSQD during the self-assembly process. We define a critical cluster size i as being one less than the number of atoms needed to form a stable nucleus. Lower stability means that more atoms are needed to form the TSQD nucleus and so i will be larger.

For homoepitaxial growth, the island size distribution scales according to a scaling function, f_i , given by^{47–49}

$$f_i(s/\langle s \rangle) = \frac{N_s(s)^2}{\theta} \quad (1)$$

where s is the size of the island, N_s is the number of islands of size s , $\langle s \rangle$ is the average island size, and θ is the coverage. The shape of f_i depends on the degree of reversibility of the adatom aggregation process, as well as on the value of i in a given system, which can take noninteger values.⁴⁸ Explicit analytic expressions for the functions f_i for integer values of i were given in ref 49. While this scaling behavior was studied in detail in the submonolayer regime, we now know that it also holds for heteroepitaxial QDs after the deposition of multiple layers.^{11,50} Researchers speculate that the scaling also holds in these cases because the heteroepitaxial TSQDs do not

coalesce and, in that sense, are somewhat similar to islands during homoepitaxy in the submonolayer, precoalescence regime.

In Figures 5 we show the scaled size distributions for Ge and GaAs TSQDs grown at $T_{\text{sub}} = 535$ °C, with different

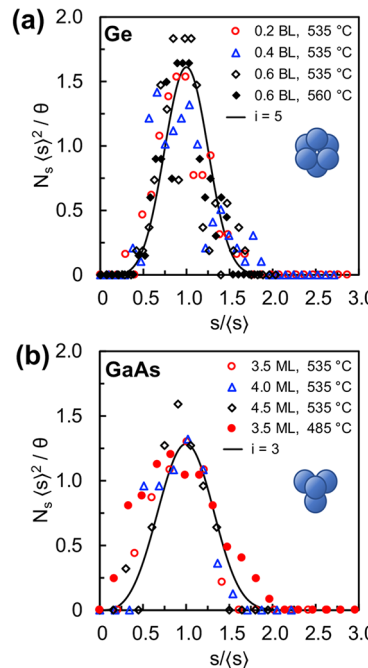


Figure 5. (a) Scaled 3D Ge/InAlAs(111)A TSQD size distributions with different Ge deposition amounts grown at $T_{\text{sub}} = 535$ and 560 °C. (b) Scaled 3D GaAs/InAlAs(111)A TSQD size distributions with different GaAs deposition amounts grown at $T_{\text{sub}} = 485$ and 535 °C. Solid lines are analytic expressions for critical cluster sizes $i = 5$ in a and $i = 3$ in b.⁴⁹ The schematics suggest how six atoms ($i = 5$) and four atoms ($i = 3$) can be arranged into clusters with 3-fold symmetry.

deposition amounts. In these plots, θ represents the effective surface coverage of the TSQDs, rather than their volume. The individual island size distributions for both the Ge and GaAs TSQDs collapse onto single curves after scaling, confirming that in each case we can describe the tensile self-assembly process with a single scaling function f_i (Figures 5a–b).

For Ge TSQDs grown at $T_{\text{sub}} = 535$ °C, the best fits to the data come from the analytic expressions for $i = 5–6$ (Figure 5a shows the fit for $i = 5$).⁴⁹ This range of values for i comes from the spread in the scaled data. When we also include scaled size distribution data for a similar Ge TSQD sample grown at $T_{\text{sub}} = 560$ °C, we see that they too lie on the $i = 5$ curve, and are essentially indistinguishable from the $T_{\text{sub}} = 535$ °C data. Therefore, at both temperatures the smallest stable cluster size (given by $i + 1$) for the Ge TSQDs consists of six atoms. That the critical cluster size appears to be insensitive to T_{sub} over this range is somewhat surprising. Previous studies of QD critical cluster sizes have found that the value of i tends to increase with T_{sub} .^{11,50} As T_{sub} rises, the additional thermal energy means that atoms are able to detach from previously stable clusters, and so for an atom to become irreversibly attached to a cluster, more atom-to-nearest-neighbor bonds are required.⁴⁹ The fact that i is the same in Figure 5a despite an increase in T_{sub} of 25 °C suggests that the six-membered TSQD nucleus is particularly stable.

Similar analysis for GaAs TSQDs grown at $T_{\text{sub}} = 535$ and 485°C results in scaled island size distributions that, regardless of T_{sub} , are best fitted with the analytic expressions for $i = 2-3$ (Figure 5b shows the fit for $i = 3$).⁴⁹ The fact that the critical cluster size for GaAs TSQD nucleation remains constant at four atoms, once again reveals that this specific arrangement is particularly stable over this 50°C range of T_{sub} .

It is worth noting that nuclei consisting of six atoms (Ge) and four atoms (GaAs) can both be arranged into clusters with 3-fold symmetries (see schematics in Figure 5a–b). For a triangular lattice, Joyce and Vvedensky referred to clusters with 3-fold symmetry as “magic” islands.⁵¹ Like them, we speculate whether clusters containing these specific numbers of Ge and Ga atoms gain additional stability by mirroring the symmetry of the underlying (111)A surface reconstruction.

D. Scaling of Ge and GaAs TSQD Radial Distributions.

Our DFT calculations predict differences in Ge and Ga adatom diffusion that we can observe experimentally. As diffusion length increases, we expect to see larger, lower density TSQDs (i.e., spaced farther apart).⁵¹ We used radial distribution analysis to explore Ge and GaAs interdot spacings and find the scaling relation $N(r)$ for their separation as a function of distance r . The radial distribution function $g(r/\langle R \rangle)$ describes the normalized probability of finding a TSQD whose center is a distance r away from the center of another^{47,52} and is given by

$$g(r/\langle R \rangle) = \frac{N(r)}{N} \quad (2)$$

where N is the TSQD areal density and $\langle R \rangle = 1/\sqrt{N}$ is the average distance between TSQDs if we assume uniform separation. Table 3 summarizes our results for $\langle R \rangle$ and the

Table 3. Experimental Values for $\langle R \rangle$ and Average TSQD Radius (r_0) for the Ge and GaAs Samples in Figures 6a–b

sample	$\langle R \rangle$ (nm)	r_0 (nm)
0.2 BL Ge, 535 °C	107 ± 14	6.4 ± 0.8
0.6 BL Ge, 535 °C	61 ± 6	8.2 ± 0.7
0.6 BL Ge, 560 °C	73.3 ± 0.4	14.9 ± 1.2
3.5 ML GaAs, 485 °C	358 ± 8	23.2 ± 5.4
4.0 ML GaAs, 535 °C	241 ± 13	32.0 ± 4.5
4.5 ML GaAs, 535 °C	360 ± 41	35.7 ± 5.3

average TSQD radius (r_0) for Ge and GaAs TSQDs grown from different deposition amounts. The values for the four samples grown at 535°C are entirely consistent with the results from our DFT calculations. At this same T_{sub} , the faster diffusion of Ga adatoms compared to Ge results in bigger GaAs TSQDs with larger average interdot separation.

For the 0.2 BL Ge TSQDs we see overlap between $\langle R \rangle = 107 \pm 14$ nm and the average InAlAs terrace width in Figure 2a of 86 ± 13 nm. The similarity between these values indicates that, at low Ge coverage, the interstep separation has a stronger influence on TSQD separation than the distance between Ge TSQDs along a given step edge. Raising the Ge coverage to 0.6 BL increases the TSQD areal density.¹⁷ As a result, $\langle R \rangle$ is reduced to 61 ± 6 nm, and so average TSQD separation along the step-edges is now less than the average InAlAs terrace width. Indeed, this is what we see from AFM images (e.g., Figure 1c in ref 17), where “chains” of QDs, often separated by less than 50 nm, decorate the step-edges. Increasing T_{sub} to 560°C enhances adatom diffusion, which

increases the average size of the 0.6 BL Ge TSQDs but reduces their density.¹⁷ As a result, $\langle R \rangle$ increases slightly to 73.3 ± 0.4 nm, but this separation is still less than the average terrace width.

Table 3 shows that raising the GaAs coverage from 3.5–4.0 ML while also raising T_{sub} from 485–535 °C has the expected combined effect of increasing average GaAs TSQD size.¹⁵ That $\langle R \rangle$ simultaneously decreases from 358–241 nm tells us that depositing an additional 0.5 ML of GaAs has a stronger effect on TSQD separation than the 50°C increase in T_{sub} which would tend to decrease areal density.¹⁵ Interestingly, raising the GaAs coverage by a further 0.5 ML at 535°C has the opposite effect on $\langle R \rangle$ of *increasing* the average TSQD separation from 241–360 nm. This decrease in TSQD areal density at high GaAs coverage is consistent with the onset of Ostwald ripening where the smallest TSQDs disappear, their material consumed by larger neighboring dots.¹⁵

Figures 6a–b show the radial distribution functions for the samples in Table 3. If TSQD nucleation was perfectly uniform,

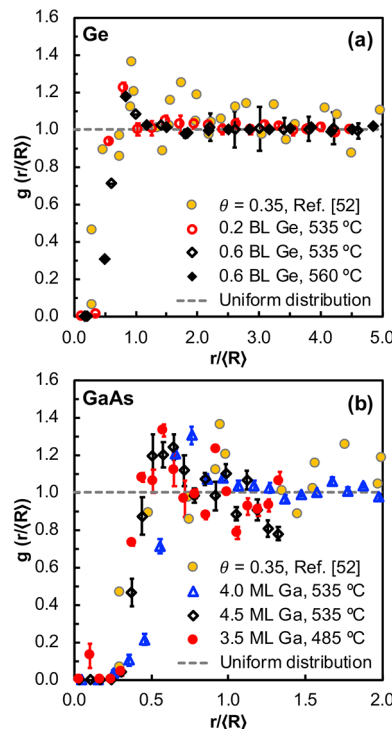


Figure 6. (a) Scaled Ge/InAlAs(111)A TSQD radial distributions with different Ge coverages grown at $T_{\text{sub}} = 535$ and 560°C . (b) Scaled GaAs/InAlAs(111)A TSQD radial distributions with different Ga coverages grown at $T_{\text{sub}} = 485$ and 535°C . In each data series, the standard errors are calculated using averages from at least three independent samples over an area of $\geq 33 \mu\text{m}^2$. Dashed lines show the uniform radial distribution for a noninteracting system. Parts a and b include comparative radial distribution data from ref 52.

their radial distributions would fall on the dashed lines at $g(r/\langle R \rangle) = 1$ in Figures 6a–b. Indeed, at long-range as $r \rightarrow \infty$ we do see $g(r/\langle R \rangle) \rightarrow 1$ as the data converge to these dashed lines. However, the fact that at short-range we see significant deviation both below and above the dashed lines indicates that the nucleation and growth of Ge and GaAs TSQDs is not uniform.

Data falling below the dashed lines tell us we have a reduced probability of finding a Ge or GaAs TSQD in very close

proximity to another. At very short-range, existing TSQDs act as local sinks for adatoms, preventing new TSQDs from nucleating nearby. Therefore, as $r \rightarrow r_0$ in Figures 6a–b, $g(r/\langle R \rangle) \rightarrow 0$.

In contrast, at slightly longer range, we see peaks in the data at $r/\langle R \rangle \sim 1$ for the Ge TSQDs, and $r/\langle R \rangle \sim 0.75$ for the GaAs TSQDs (Figures 6a–b). Data above the dashed lines at $g(r/\langle R \rangle) > 1$ are a measure of how many times more likely a TSQD is to be found at distance $r/\langle R \rangle$ from the center of any other TSQD. The peaks in the data therefore reveal spatial correlations for both Ge and GaAs TSQDs. We attribute the appearance of these peaks to the fact that existing TSQDs are surrounded by a capture zone for adatoms within which new TSQDs cannot nucleate. The result is an effective “repulsion” between the TSQD centers above a critical nucleus size. This is supported by simulation results for strained island growth in the submonolayer regime.^{53,54} The island size distribution narrows and sharpens as a function of strain, because the island capture zones become more regular.

After sampling at least $31\ 1\ \mu\text{m}^2$ areas for each radial distribution function, these peaks of height $g(r/\langle R \rangle) = 1.2\text{--}1.4$ for Ge and GaAs TSQDs show good agreement with the correlation peaks of ~ 1.4 observed by Bressler-Hill et al. for distributions of InAs/GaAs(001) QDs (see yellow circles in Figures 6a–b).⁵² It is noteworthy that despite the opposite sign of strain, these similarities suggest tensile-strained Ge and GaAs QDs exhibit nearly identical spatial distributions and capture zones of comparable strength to traditional compressively strained InAs/GaAs(001) QDs.⁵² This is the first demonstration of tensile-strained QDs distributed with a preferred separation. In the future, the use of similar studies to tune short-range separations of Ge and GaAs TSQDs could be quite attractive for tailoring quantum dot densities to specific optoelectronic applications.

It is noteworthy that we do not observe temperature-dependent differences in the radial distribution functions for either Ge or GaAs TSQDs. The general agreement (to within error) of the various data sets in Figure 6a–b suggest that the observed spatial correlations of the Ge and GaAs TSQDs persist across the T_{sub} ranges explored here.

V. CONCLUSION

Although Ge and GaAs TSQDs both self-assemble on $\text{In}_{0.52}\text{Al}_{0.48}\text{As}(111)\text{A}$ surfaces, their structural characteristics (size, shape, and areal density) are quite different. Formation of these TSQDs can be reproduced reliably over a fairly broad range of substrate temperatures. It appears that the critical island size for both Ge and GaAs TSQD nucleation is unchanged over the temperature windows explored here, enabling robust control of TSQD size uniformity and areal density. Our DFT calculations predict that regardless of the surface reconstruction, Ga diffuses much faster on the $\text{In}_{0.52}\text{Al}_{0.48}\text{As}(111)\text{A}$ surface than Ge. These DFT results are borne out experimentally, as we show that Ge TSQDs are smaller and higher density than GaAs TSQDs grown at the same substrate temperature. We speculate that while GaAs clusters are stable enough to form on the terraces, most Ge clusters form at step-edges as a result of the extra stability provided by the additional dangling bonds. We find experimental support for this hypothesis from island size scaling analysis of our TSQD data, which shows that more atoms are required to form a stable Ge nucleus than a GaAs nucleus. The spatial distributions of Ge and GaAs TSQDs are

not uniform. Instead we see that the TSQDs are distributed such that they have a preferred separation from one another and that these spatial correlations are independent of substrate temperature over the ranges studied here. To build on these results, we are planning a more detailed DFT study of the binding energies and stability of step edges. The insights gained from this study will assist researchers interested in designing Ge(111) and GaAs(111)A TSQD arrays for a range of applications from novel infrared emitters to entangled photon sources.

■ AUTHOR INFORMATION

Corresponding Author

Paul J. Simmonds – *Micron School of Materials Science & Engineering and Department of Physics, Boise State University, Boise, Idaho 83725, United States;*  orcid.org/0000-0001-5524-0835; Email: paulsimmonds@boisestate.edu

Authors

Kathryn E. Sautter – *Micron School of Materials Science & Engineering, Boise State University, Boise, Idaho 83725, United States;*  orcid.org/0000-0003-1173-343X

Christopher F. Schuck – *Micron School of Materials Science & Engineering, Boise State University, Boise, Idaho 83725, United States*

Justin C. Smith – *Department of Mathematics, University of California, Los Angeles, California 90095, United States*

Kevin D. Vallejo – *Micron School of Materials Science & Engineering, Boise State University, Boise, Idaho 83725, United States*

Trent A. Garrett – *Department of Physics, Boise State University, Boise, Idaho 83725, United States*

Jake Soares – *Micron School of Materials Science & Engineering, Boise State University, Boise, Idaho 83725, United States*

Hunter J. Coleman – *Department of Physics, Boise State University, Boise, Idaho 83725, United States*

Michael M. Henry – *Micron School of Materials Science & Engineering, Boise State University, Boise, Idaho 83725, United States;*  orcid.org/0000-0002-3870-9993

Eric Jankowski – *Micron School of Materials Science & Engineering, Boise State University, Boise, Idaho 83725, United States;*  orcid.org/0000-0002-3267-1410

Christian Ratsch – *Department of Mathematics, University of California, Los Angeles, California 90095, United States; Institute for Pure and Applied Mathematics, University of California, Los Angeles, California 90095, United States*

Complete contact information is available at:

<https://pubs.acs.org/10.1021/acs.cgd.0c01528>

Author Contributions

¹K.E.S. and C.F.S. contributed equally to this work.

Notes

The authors declare no competing financial interest.

The data that support the findings of this study are available from the corresponding author upon reasonable request.

■ ACKNOWLEDGMENTS

This material is based upon work supported by the Air Force Office of Scientific Research under award number FA9550-16-1-0278 and by the National Science Foundation under NSF

CAREER Grant No. 1555270. We acknowledge Elton Graugnard and Steven M. Hues (Boise State University) for valuable assistance with XPS. AFM was done at the Boise State Surface Science Laboratory.

■ REFERENCES

- (1) Richardella, A.; Zhang, D. M.; Lee, J. S.; Koser, A.; Rench, D. W.; Yeats, A. L.; Buckley, B. B.; Awschalom, D. D.; Samarth, N. Coherent heteroepitaxy of Bi_2Se_3 on GaAs (111)B. *Appl. Phys. Lett.* **2010**, *97*, 262104.
- (2) He, L.; Xiu, F.; Wang, Y.; Fedorov, A. V.; Huang, G.; Kou, X.; Lang, M.; Beyermann, W. P.; Zou, J.; Wang, K. L. Epitaxial growth of Bi_2Se_3 topological insulator thin films on Si (111). *J. Appl. Phys.* **2011**, *109*, 103702.
- (3) Guo, X.; Xu, Z. J.; Liu, H. C.; Zhao, B.; Dai, X. Q.; He, H. T.; Wang, J. N.; Liu, H. J.; Ho, W. K.; Xie, M. H. Single domain Bi_2Se_3 films grown on InP(111)A by molecular-beam epitaxy. *Appl. Phys. Lett.* **2013**, *102*, 151604.
- (4) Vishwanath, S.; Liu, X.; Rouvimov, S.; Basile, L.; Lu, N.; Azcatl, A.; Magno, K.; Wallace, R. M.; Kim, M.; Idrobo, J.-C.; Furdyna, J. K.; Jena, D.; Xing, H. G. Controllable growth of layered selenide and telluride heterostructures and superlattices using molecular beam epitaxy. *J. Mater. Res.* **2016**, *31*, 900–910.
- (5) May, B. J.; Hettiaratchy, E. C.; Myers, R. C. Controlled nucleation of monolayer MoSe_2 islands on Si (111) by MBE. *J. Vac. Sci. Technol., B: Nanotechnol. Microelectron.: Mater., Process., Meas., Phenom.* **2019**, *37*, 021211.
- (6) Yuan, X.; Tang, L.; Liu, S.; Wang, P.; Chen, Z.; Zhang, C.; Liu, Y.; Wang, W.; Zou, Y.; Liu, C.; Guo, N.; Zou, J.; Zhou, P.; Hu, W.; Xiu, F. Arrayed van der Waals vertical heterostructures based on 2D GaSe grown by molecular beam epitaxy. *Nano Lett.* **2015**, *15*, 3571–3577.
- (7) Caridi, E. A.; Chang, T. Y.; Goossen, K. W.; Eastman, L. F. Direct demonstration of a misfit strain-generated electric field in a [111] growth axis zinc-blende heterostructure. *Appl. Phys. Lett.* **1990**, *56*, 659–661.
- (8) David, J. P. R.; Sale, T. E.; Pabla, A. S.; Rodríguez-Gironés, P. J.; Woodhead, J.; Grey, R.; Rees, G. J.; Robson, P. N.; Skolnick, M. S.; Hogg, R. A. *Mater. Sci. Eng., B* **1995**, *35*, 42–46.
- (9) Mehratra, S. R.; Povolotskyi, M.; Elias, D. C.; Kubis, T.; Law, J. M.; Rodwell, M. J. W.; Klimeck, G. Simulation study of thin-body ballistic n-MOSFETs involving transport in mixed Γ -L valleys. *IEEE Electron Device Lett.* **2013**, *34*, 1196–1198.
- (10) Alam, K.; Takagi, S.; Takenaka, M. Strain-modulated L-valley ballistic-transport in (111) GaAs ultrathin-body nMOSFETs. *IEEE Trans. Electron Devices* **2014**, *61*, 1335–1340.
- (11) Simmonds, P. J.; Lee, M. L. Self-assembly on (111)-oriented III-V surfaces. *Appl. Phys. Lett.* **2011**, *99*, 123111.
- (12) Simmonds, P. J.; Lee, M. L. Tensile-strained growth on low-index GaAs. *J. Appl. Phys.* **2012**, *112*, 054313.
- (13) Yerino, C. D.; Simmonds, P. J.; Liang, B.; Dorogan, V. G.; Ware, M. E.; Mazur, Y. I.; Jung, D.; Huffaker, D. L.; Salamo, G. J.; Lee, M. L. Tensile GaAs(111) quantum dashes with tunable luminescence below the bulk bandgap. *Appl. Phys. Lett.* **2014**, *105*, 071912.
- (14) Yerino, C. D.; Simmonds, P. J.; Liang, B.; Jung, D.; Schneider, C.; Unsleber, S.; Vo, M.; Huffaker, D. L.; Hofling, S.; Kamp, M.; Lee, M. L. Strain-driven growth of GaAs(111) quantum dots with low fine structure splitting. *Appl. Phys. Lett.* **2014**, *105*, 251901.
- (15) Schuck, C. F.; McCown, R. A.; Hush, A.; Mello, A.; Roy, S.; Spinuzzi, J. W.; Liang, B.; Huffaker, D. L.; Simmonds, P. J. Self-assembly of (111)-oriented tensile-strained quantum dots by molecular beam epitaxy. *J. Vac. Sci. Technol., B: Nanotechnol. Microelectron.: Mater., Process., Meas., Phenom.* **2018**, *36*, 031803.
- (16) Schuck, C. F.; Roy, S. K.; Garrett, T.; Yuan, Q.; Wang, Y.; Cabrera, C. I.; Grossklaus, K. A.; Vandervelde, T. E.; Liang, B.; Simmonds, P. J. Anomalous Stranski-Krastanov growth of (111)-oriented quantum dots with tunable wetting layer thickness. *Sci. Rep.* **2019**, *9*, 18179.
- (17) Sautter, K. E.; Schuck, C. F.; Garrett, T. A.; Weltner, A. E.; Vallejo, K. D.; Ren, D.; Liang, B.; Grossklaus, K. A.; Vandervelde, T. E.; Simmonds, P. J. Self-assembly of tensile-strained Ge quantum dots on InAlAs(111)A. *J. Cryst. Growth* **2020**, *533*, 125468.
- (18) Niquet, Y.; Rideau, D.; Tavernier, C.; Jaouen, H.; Blase, X. Onsite matrix elements of the tight-binding Hamiltonian of a strained crystal: Application to silicon, germanium, and their alloys. *Phys. Rev. B: Condens. Matter Mater. Phys.* **2009**, *79*, 245201.
- (19) El Kurdi, M.; Fishman, G.; Sauvage, S.; Boucaud, P. Band structure and optical gain of tensile-strained germanium based on a 30 band k-p formalism. *J. Appl. Phys.* **2010**, *107*, 013710.
- (20) Yang, C.; Yu, Z.; Liu, Y.; Lu, P.; Gao, T.; Li, M.; Manzoor, S. Dependence of electronic properties of germanium on the in-plane biaxial tensile strains. *Phys. B (Amsterdam, Neth.)* **2013**, *427*, 62–67.
- (21) Simmonds, P. J.; Yerino, C. D.; Sun, M.; Liang, B.; Huffaker, D. L.; Dorogan, V. G.; Mazur, Y.; Salamo, G.; Lee, M. L. Tuning Quantum Dot Luminescence Below the Bulk Band Gap Using Tensile Strain. *ACS Nano* **2013**, *7*, 5017–5023.
- (22) Vrijen, R.; Yablonovitch, E. A spin-coherent semiconductor photo-detector for quantum communication. *Phys. E* **2001**, *10*, 569–575.
- (23) Huo, Y. H.; et al. A light-hole exciton in a quantum dot. *Nat. Phys.* **2014**, *10*, 46–51.
- (24) Juska, G.; Dimastropoulos, V.; Mereni, L. O.; Gocalinska, A.; Pelucchi, E. Towards quantum-dot arrays of entangled photon emitters. *Nat. Photonics* **2013**, *7*, 527–531.
- (25) Stock, E.; Warming, T.; Ostapenko, I.; Rodt, S.; Schliwa, A.; Töfflinger, J.; Lochmann, A.; Toropov, A.; Moshchenko, S.; Dmitriev, D.; Haisler, V.; Bimberg, D. Single-photon emission from InGaAs quantum dots grown on (111) GaAs. *Appl. Phys. Lett.* **2010**, *96*, 093112.
- (26) Yerino, C. D.; Liang, B.; Huffaker, D. L.; Simmonds, P. J.; Lee, M. L. Review Article: Molecular beam epitaxy of lattice-matched InAlAs and InGaAs layers on InP(111)A, (111)B, and (110). *J. Vac. Sci. Technol., B: Nanotechnol. Microelectron.: Mater., Process., Meas., Phenom.* **2017**, *35*, 010801.
- (27) Sadeghi, I.; Tam, M. C.; Wasilewski, Z. R. On the optimum off-cut angle for the growth on InP(111)B substrates by molecular beam epitaxy. *J. Vac. Sci. Technol., B: Nanotechnol. Microelectron.: Mater., Process., Meas., Phenom.* **2019**, *37*, 031210.
- (28) Schuck, C. F.; Vallejo, K. D.; Garrett, T.; Yuan, Q.; Wang, Y.; Liang, B.; Simmonds, P. J. Impact of arsenic species on self-assembly of triangular and hexagonal tensile-strained GaAs(111)A quantum dots. *Semicond. Sci. Technol.* **2020**, *35*, 105001.
- (29) Schneider, C. A.; Rasband, W. S.; Eliceiri, K. W. NIH Image to ImageJ: 25 years of image analysis. *Nat. Methods* **2012**, *9*, 671–675.
- (30) Ramasubramani, V.; Dice, B. D.; Harper, E. S.; Spellings, M. P.; Anderson, J. A.; Glotzer, S. C. freud: A Software Suite for High Throughput Analysis of Particle Simulation Data. *arXiv.org* **2019**, No. 1906.06317.
- (31) Hohenberg, P.; Kohn, W. Inhomogeneous Electron Gas. *Phys. Rev.* **1964**, *136*, B864–B871.
- (32) Kohn, W.; Sham, L. J. Self-Consistent Equations Including Exchange and Correlation Effects. *Phys. Rev.* **1965**, *140*, A1133–A1138.
- (33) Blum, V.; Gehrke, R.; Hanke, F.; Havu, P.; Havu, V.; Ren, X.; Reuter, K.; Scheffler, M. Ab initio molecular simulations with numeric atom-centered orbitals. *Comput. Phys. Commun.* **2009**, *180*, 2175–2196.
- (34) Havu, V.; Blum, V.; Havu, P.; Scheffler, M. Efficient O(N) integration for all-electron electronic structure calculation using numeric basis functions. *J. Comput. Phys.* **2009**, *228*, 8367–8379.
- (35) Marek, A.; Blum, V.; Johann, R.; Havu, V.; Lang, B.; Auckenthaler, T.; Heinecke, A.; Bungartz, H.-J.; Lederer, H. The ELPA library: scalable parallel eigenvalue solutions for electronic structure theory and computational science. *J. Phys.: Condens. Matter* **2014**, *26*, 213201.

- (36) Yu, V. W.-z.; Corsetti, F.; Garcia, A.; Huhn, W. P.; Jacquelin, M.; Jia, W.; Lange, B.; Lin, L.; Lu, J.; Mi, W.; Seifitokaldani, A.; Vazquez-Mayagoitia, A.; Yang, C.; Yang, H.; Blum, V. ELSI: A unified software interface for Kohn-Sham electronic structure solvers. *Comput. Phys. Commun.* **2018**, *222*, 267–285.
- (37) Perdew, J. P.; Burke, K.; Ernzerhof, M. Generalized gradient approximation made simple. *Phys. Rev. Lett.* **1996**, *77*, 3865.
- (38) Zunger, A.; Wei, S.-H.; Ferreira, L. G.; Bernard, J. E. Special quasirandom structures. *Phys. Rev. Lett.* **1990**, *65*, 353.
- (39) Wei, S.-H.; Ferreira, L. G.; Bernard, J. E.; Zunger, A. Electronic properties of random alloys: Special quasirandom structures. *Phys. Rev. B: Condens. Matter Mater. Phys.* **1990**, *42*, 9622.
- (40) Moison, J. M.; Guille, C.; Houzay, F.; Barthe, F.; Van Rompay, M. Surface segregation of third-column atoms in group III-V arsenide compounds: Ternary alloys and heterostructures. *Phys. Rev. B: Condens. Matter Mater. Phys.* **1989**, *40*, 6149–6162.
- (41) Houzay, F.; Moison, J.M.; Guille, C.; Barthe, F.; Van Rompay, M. Surface segregation of third-column atoms in III-V ternary arsenides. *J. Cryst. Growth* **1989**, *95*, 35–37.
- (42) Moll, N.; Kley, A.; Pehlke, E.; Scheffler, M. GaAs equilibrium crystal shape from first principles. *Phys. Rev. B: Condens. Matter Mater. Phys.* **1996**, *54*, 8844–8855.
- (43) Peters, B.; Heyden, A.; Bell, A. T.; Chakraborty, A. A growing string method for determining transition states: Comparison to the nudged elastic band and string methods. *J. Chem. Phys.* **2004**, *120*, 7877–7886.
- (44) Henkelman, G.; Uberuaga, B. P.; Jonsson, H. A climbing image nudged elastic band method for finding saddle points and minimum energy paths. *J. Chem. Phys.* **2000**, *113*, 9901–9904.
- (45) Eisele, H.; Lenz, A.; Heitz, R.; Timm, R.; Dähne, M.; Temko, Y.; Suzuki, T.; Jacobi, K. Change of InAs/GaAs quantum dot shape and composition during capping. *J. Appl. Phys.* **2008**, *104*, 124301.
- (46) Shapiro, J. N.; Lin, A.; Huffaker, D. L.; Ratsch, C. Potential energy surface of In and Ga adatoms above the (111)A and (110) surfaces of a GaAs nanopillar. *Phys. Rev. B: Condens. Matter Mater. Phys.* **2011**, *84*, 085322.
- (47) Bartelt, M. C.; Evans, J. W. Scaling analysis of diffusion-mediated island growth in surface adsorption processes. *Phys. Rev. B: Condens. Matter Mater. Phys.* **1992**, *46*, 12675–12687.
- (48) Ratsch, C.; Šmilauer, P.; Zangwill, A.; Vvedensky, D. D. Submonolayer epitaxy without a critical nucleus. *Surf. Sci.* **1995**, *329*, L599–L604.
- (49) Amar, J. G.; Family, F. Critical Cluster Size: Island Morphology and Size Distribution in Submonolayer Epitaxial Growth. *Phys. Rev. Lett.* **1995**, *74*, 2066–2069.
- (50) Krzyzewski, T. J.; Joyce, P. B.; Bell, G. R.; Jones, T. S. Scaling behavior in InAs/GaAs(001) quantum-dot formation. *Phys. Rev. B: Condens. Matter Mater. Phys.* **2002**, *66*, No. 201302(R).
- (51) Joyce, B.; Vvedensky, D. Self-organized growth on GaAs surfaces. *Mater. Sci. Eng., R* **2004**, *46*, 127–176.
- (52) Bressler-Hill, V.; Varma, S.; Lorke, A.; Noshio, B. Z.; Petroff, P. M.; Weinberg, W. H. Island Scaling in Strained Heteroepitaxy: InAs/GaAs(001). *Phys. Rev. Lett.* **1995**, *74*, 3209–3212.
- (53) Ratsch, C.; Zangwill, A.; Šmilauer, P. Scaling of heteroepitaxial island sizes. *Surf. Sci.* **1994**, *314*, L937.
- (54) Ratsch, C.; DeVita, J.; Smereka, P. Level-set simulation for the strain-driven sharpening of the island-size distribution during submonolayer heteroepitaxial growth. *Phys. Rev. B: Condens. Matter Mater. Phys.* **2009**, *80*, 155309.